RSC Advances

PAPER

View Article Online
View Journal | View Issue

Cite this: *RSC Adv.*, 2022, **12**, 22526

TiO_2 nanoparticles decorated with Co-Schiff base-g-C_3N_4 as an efficient photocatalyst for one-pot visible light-assisted synthesis of benzimidazoles†

Narges Pourmorteza, Maasoumeh Jafarpour, * Fahimeh Feizpour and Abdolreza Rezaeifard *

In this study, a novel heterogeneous visible light-driven nanocatalyst was produced *via* the complexation of Co(II) with g-C_3N_4-imine-functionalized TiO_2 nanoparticles. It was characterized using different techniques such as Fourier-transform infrared (FT-IR), energy-dispersive X-ray spectrum (EDS), inductively coupled plasma atomic emission spectroscopy (ICP-AES), thermogravimetric analysis (TGA), ultraviolet-visible diffuse reflectance spectroscopy (UV-vis DRS), X-ray diffraction (XRD), and scanning electron microscopy (SEM). The catalyst promoted several different transformations in a one-pot reaction sequence: aerobic photooxidation of benzylic alcohols to aldehydes and then the tandem synthesis of benzimidazoles through the dehydrogenative coupling of primary benzylic alcohols and aromatic diamines. The photocatalyst proved to be highly active, robust, selective, and recyclable under organic reaction conditions and provided affordable products with good to high yields. The results proposed that the improved photoactivity predominantly benefits from the synergistic effects of the heterojunction of Co-carbon nitride on TiO_2 nanoparticles. Moreover, this protocol provides standard conditions avoiding undesirable additives and limitations of oxidation methods, and may help to develop a new strategy for the development of photocatalysis based organic transformations.

Received 28th April 2022
Accepted 13th July 2022

DOI: 10.1039/d2ra02699f

rsc.li/rsc-advances

1 Introduction

From the viewpoint of green and sustainable chemistry, the use of a renewable source of energy for evolving efficient and economical chemical processes has attracted extensive attention.[1] In this line, semiconductor photocatalysis is highly expected to provide a sustainable pathway for the green synthesis and technology because of its potential utilization for clean and safe solar energy in the past few years.[2–4] A significantly efficient, stable, affordable, and easily separable semiconductor material that is capable of light harvesting is also an essential prerequisite for the economical use of catalysts. Among them, titanium dioxide adopts an application-driven perspective with unique properties that have long been employed.[5–8] Nevertheless, the wide band-gap (about 3.2 eV) and the high recombination rate of photoinduced electron–holes are the main drawbacks that give rise to poor photocatalytic activity under visible light irradiation.[9,10] Therefore, the development of highly active visible-light photocatalysts will always be a global research direction.

More recently, a new type of polymeric semiconductor, graphitic CN (g-C_3N_4), has grabbed extensive attention because of its appealing electronic structure, metal-free property, large scale preparation, low cost, and visible light adsorption (2.7 eV), which results in tunable band gap due to the ease of chemical functionalization and doping methods.[11–16] These distinct characteristics endow it a novel and unique nature in photocatalysis and exhibit promising properties toward multifaceted applications such as solar energy conversion,[17] water splitting,[18] and sustainable hydrogen production.[19] Despite these priorities, the photocatalytic activity of pure g-C_3N_4 is still limited due to low visible-light utilization efficiency and low specific surface area.[20,21] To address these problems, many methods have been exploited, including chemical doping with nonmetal or metal elements, morphology, pore structure design, protonation, and building heterostructures.[22–26] Among them, constructing heterostructures by combining g-C_3N_4 with other appropriate semiconductors is considered an effective method for improving its photocatalytic activity and enhanced quantum efficiency.[27–30] One of these investigations has been devoted to hybrids of g-C_3N_4 with TiO_2, which used visible light more effectively.[31]

The photocatalysis of organic synthesis has been recognized as an imperative research area in photochemistry in the past two decades.[32–34] Photocatalytic reactions can be categorized as a "green" science since it allows chemical transformations

Catalysis Research Laboratory, Department of Chemistry, Faculty of Science, University of Birjand, Birjand, 97179-414, Iran. E-mail: mjafarpour@birjand.ac.ir; rrezaeifard@birjand.ac.ir; Fax: +98 561 322202515; Tel: +98 561 32202516

† Electronic supplementary information (ESI) available. See https://doi.org/10.1039/d2ra02699f

under light irradiation as an environment-friendly synthetic route.[35,36] The method described herein, in comparison to the commercially used synthetic methods that rely on the use of expensive and hazardous reagents, and cause generation by-products, is cost-effective, highly selective, and ecofriendly. Benzimidazoles, which are known as the main building blocks in the structures of pharmaceuticals, natural products, functional materials, and agrochemical compounds, have grabbed considerable attention in organic synthesis in recent decades.[7,37] Among the reported methods used for the synthesis of benzimidazoles, the use of alcohols as a starting material is a plausible alternative, considering the economic viability and environmental integrity due to the wide accessibility of alcohols.[38–46]

In this line of research and during our efforts on the development of innovative and ecofriendly nanophotocatalysts for sustainable chemical processes, herein, we present a new visible-light photocatalyst by building the heterostructure of nanocrystalline TiO_2 with cobalt-carbon nitride imine complex. The catalyst demonstrated an efficient and environment-friendly method for the aerobic photooxidation of benzylic alcohols to aldehydes and then the synthesis of benzimidazole derivatives, followed by coupling with aromatic diamines in a second reaction process (Scheme 1). Subsequently, the possibility of using benzaldehydes as commonly used starting materials for condensation with 1,2-diaminobenzenes for the synthesis of benzimidazoles is also described. An additional advantage of this catalytic system is its sustainable stability under oxidative conditions and reusability of at least five runs.

2 Experimental

Note: see the step-by-step preparation of the g-C_3N_4-imine/TiO_2 nanohybrid in the ESI.†[47]

2.1 Preparation of the Co-g-C_3N_4-imine/TiO_2 nanohybrid

First, 0.1 g TiO_2 nanoparticles were gradually added to 0.1 g Schiff base of carbon nitride in ethanol at 60 °C under ultrasonic agitation. Then, the as-obtained mixture was refluxed for 8 h. Thus, the product was centrifuged and washed with ethanol. Finally, g-C_3N_4-imine/TiO_2 nanocomposite was obtained after drying in air. Subsequently, to load Co on the surface of g-C_3N_4-imine/TiO_2 heterostructure, $Co(OAc)_2$ suspension (6 mg per mL ethanol) was added to 0.1 g g-C_3N_4-imine/TiO_2 dispersed in 2 mL ethanol. After sonication for 1 h, the mixture was refluxed for 3 h. The grey participants were collected by centrifuging and washed with ethanol repeatedly and dried in air.

2.2 Typical procedure for the aerobic oxidation of benzyl alcohols

To a mixture of benzyl alcohols (0.125 mmol) and NHPI (*N*-hydroxyphthalimide) (0.012 mmol, 2 mg) in CH_3CN (0.5 mL), Co-g-C_3N_4-imine/TiO_2 nanocatalyst (0.5 mol%, 2 mg) was added, and the reaction mixture was stirred at 70 °C under air and CFL lamp as a source of visible light for the required time. The reaction progress was monitored by GC analysis, and the yields of the products were determined by GC and NMR analysis.

2.3 Typical procedure for the one-pot synthesis of benzimidazole from benzyl alcohols and 1,2-phenylenediamines

To a mixture of benzyl alcohol (0.12 mmol) and NHPI (0.012 mmol, 2 mg) in CH_3CN (0.5 mL) in a glass test tube (10 cm tall × 1 cm diameter), Co-g-C_3N_4 Imine/TiO_2 nanocatalyst (3 mg) was added, and the reaction mixture was heated at 70 °C under air and CFL lamp as a source of visible light. After a few minutes, 1,2-phenylenediamine (0.15 mmol) was added. The reaction progress was monitored by TLC (eluent *n*-hexane : EtOAc, 1.5 : 1). After the completion of the reaction, the mixture was cooled to room temperature and the nanocatalyst was separated by centrifugation, followed by decantation (3 × 5 mL ethanol). The desired product (liquid phase) was purified by plate chromatography and eluted with *n*-hexane : EtOAc (10 : 2). The assignments of the products were made by the ^1H NMR spectral data and compared with the authentic samples.

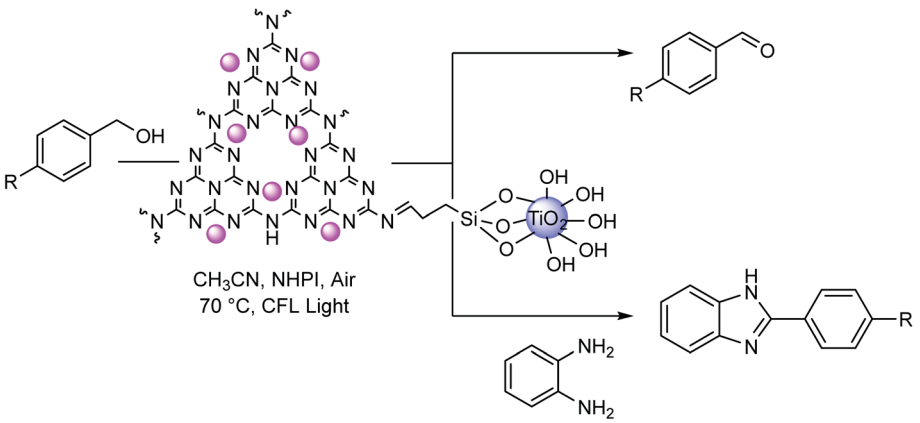

Scheme 1 Co-g-C_3N_4-imine/TiO_2 nanohybrid-catalyzed selective aerobic oxidation of alcohols and one-pot synthesis of benzimidazoles.

2.4 Typical procedure for the synthesis of benzimidazole from benzaldehydes and 1,2-phenylenediamines

To a mixture of benzaldehydes (0.125 mmol) and 1,2-phenylenediamine (0.15 mmol) in EtOH (0.5 mL) in a glass test tube (10 cm tall × 1 cm diameter), Co-g-C_3N_4 Imine/TiO_2 nanocatalyst (2 mg) was added, and the reaction mixture was heated at 60 °C under air and CFL lamp as a source of visible light for the required time. The reaction progress was monitored by TLC (eluent *n*-hexane : EtOAc, 1.5 : 1). After the completion of the reaction, the mixture was cooled to room temperature and the nanocatalyst was separated by centrifugation, followed by decantation (3 × 5 mL ethanol). The desired product (liquid phase) was purified by plate chromatography eluted with *n*-hexane : EtOAc (10 : 2). The assignments of the products were made by ^{1}H NMR spectral data in comparison with the authentic samples.

3 Results and discussion

3.1 Catalyst characterization

At the first step of this investigation, TiO_2 nanoparticles and g-C_3N_4 (ref. 47) were prepared by following the reported procedures with minor modifications. Then, g-C_3N_4/Imine organosilicon compound was synthesized with the condensation of the –NH_2 group of g-C_3N_4 with organosilicon aldehyde, which was prepared by our group.[48] Subsequently, g-C_3N_4/Imine compound was attached to TiO_2, which gave the g-C_3N_4-imine/TiO_2 nanostructure. Finally, the desired cobalt-containing catalyst (Co-g-C_3N_4-imine/TiO_2) was obtained by incorporating $Co(OAc)_2$ into g-C_3N_4-imine/TiO_2 under sonication and reflux conditionx (Scheme S1†) (for experimental details, see the ESI†).

FT-IR spectroscopy was applied to identify the bonding structure and composition of Co-g-C_3N_4-imine/TiO_2 nanocatalyst. As shown in Fig. 1, the comparison of the FT-IR spectra of TiO_2 (a), g-C_3N_4 (b), g-C_3N_4-imine/TiO_2 (c) with Co-g-C_3N_4-imine/TiO_2 nanohybrid (d) confirmed the successful fabrication of the catalyst. The presence of a typical band for TiO_2 at 450–750 cm^{-1} observed in the spectra (a, c and d) is attributed to the stretching vibrations of the Ti–O groups.[49] Moreover, the corresponding O–H bands and surface adsorbed water are also observed at 1625 and 3400 cm^{-1} regions.[50] In the spectrum of pure g-C_3N_4 (Fig. 1b), the sharp absorption band at 810 cm^{-1} indicates the typical breathing mode of the triazine ring system, while a series of bands for the stretching vibrations of C–N and C=N bonds in the heterocycles appeared in the 1242–1634 cm^{-1} region.[51] As seen in Fig. 1c, the strong absorption peaks at 1000–1130 cm^{-1} can be ascribed to the Si–O bands' stretching vibration mode.[48] Besides, the characteristic peaks of g-C_3N_4 and TiO_2 appeared in Fig. 1c and d, confirming their presence in the as-prepared composite.

The as-prepared Co-g-C_3N_4-imine/TiO_2 nanohybrid was analyzed by ICP-AES, and the Co loading was found to be 1.63 mmol g^{-1}.

The scanning electron microscopy (SEM) image was taken to characterize the structure of the composite. The morphology and size distribution of the Co-g-C_3N_4-imine/TiO_2 nanohybrid revealed a spherical morphology with sizes in the range of 19–23 nm (Fig. 2).

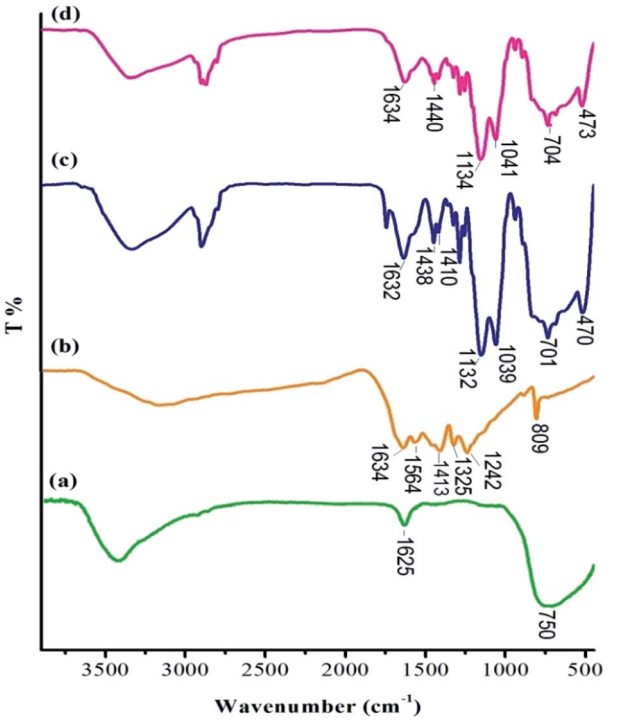

Fig. 1 FT-IR spectra of (a) nanostructure TiO_2, (b) g-C_3N_4, (c) g-C_3N_4-imine/TiO_2, (d) Co-g-C_3N_4-imine/TiO_2 nanohybrid.

The elemental mapping at the microstructural level by SEM with energy-dispersive X-ray spectrum (EDS) is given in Fig. S1.† It shows that the Ti, O, Si, N, and Co elements exist in the composited material with homogeneous distribution. The crystallinity and phase structures of the synthesized materials were determined by XRD analysis (Fig. 3). The obvious diffraction peaks at 2θ values of 25.4°, 37.7°, 48.2°, and 54.1° corresponded to the (101), (004), (200), and (105) planes of TiO_2, clearly suggesting that TiO_2 can be assigned to the anatase phase [JCPDS no. 21-1272] (Fig. 3a). Two diffraction peaks of g-C_3N_4 revealed an intense peak at the 2θ of 27.4° and 13.1°, indexed to (002) and (100) planes, respectively, which matched well with JCPDS no 87-1526. This diffraction appeared due to the stacked structure of graphite-like conjugated triazine units (Fig. 3b). As seen in Fig. 3c, the g-C_3N_4-imine/TiO_2 composite showed similar diffraction patterns to the g-C_3N_4 and TiO_2 nanoparticle, which indicated that the framework structure of the nanohybrid remained intact after modifying procedure. Also, the peak at 22.5° is ascribed to SiO_2 in the heterostructure. For Co-g-C_3N_4-imine/TiO_2, the XRD pattern also reveals the coexistence of phase structures after the process. In Fig. 3d, the intensity of the peak was reduced, which is most likely due to the intercalation of cobalt between the sheets of graphitic carbon nitride and its low loading.

To investigate the optical properties of TiO_2, g-C_3N_4, g-C_3N_4-imine, g-C_3N_4-imine/TiO_2, and Co-g-C_3N_4-imine/TiO_2 composites,the UV-vis diffuse reflectance spectra (DRS) and Tauc plots

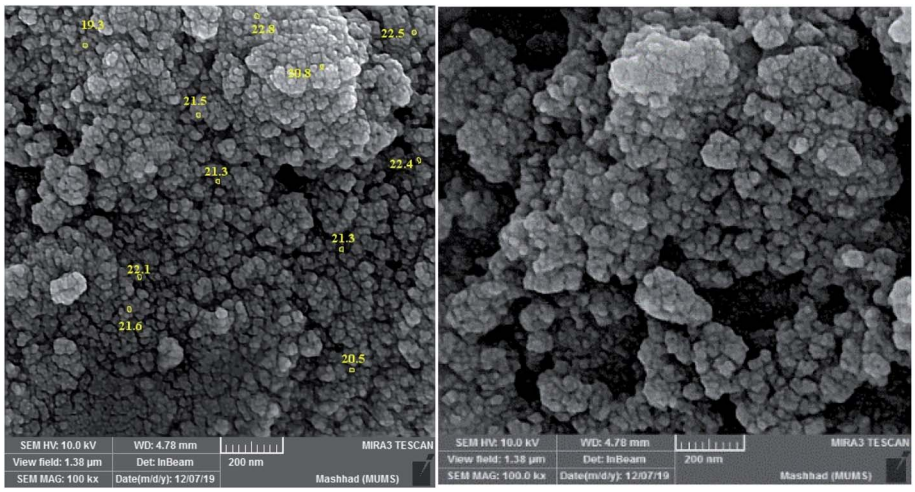

Fig. 2 SEM images of the Co-g-C_3N_4-imine/TiO_2 nanohybrid.

were recorded (Fig. 4 and S2†). In comparison with other samples, Co-g-C_3N_4-imine/TiO_2 demonstrates a significant enhancement in visible light absorption. Furthermore, there is a new absorption band present between 400 and 800 nm for the Co-g-C_3N_4-imine/TiO_2 sample, which means that absorption onset was extended into the visible light region and confirmed the photocatalytic activity of the nanohybrid. Also, band gap values based on Tauc plots showed TiO_2, g-C_3N_4, g-C_3N_4-imine, g-C_3N_4-imine/TiO_2, and Co-g-C_3N_4-imine/TiO_2 at ~3.15, 2.7, 2.9, 3, and 2.8 eV, respectively. Thus, the Co-g-C_3N_4-imine/TiO_2 semiconductor material with a relatively narrow band gap can have a strong absorption of visible light and effectively promote subsequent photocatalytic reactions.

Thermogravimetric studies were done in the temperature range of 25–900 °C. The thermal decomposition curve of the nanohybrid showed a sequence of three decomposition steps, as shown in Fig. S3.† The first decomposition step for the Co-g-C_3N_4-imine/TiO_2 nanohybrid occurred in the temperature range of 25–140 °C, which corresponds to the removal of physically adsorbed water and solvent molecules. The second step is due to the decomposition of organosilicon molecules present in the nanohybrid (240–350 °C), which can be attributed to the breakdown of the g-C_3N_4-imine. A 23% weight loss in the temperature range of 350−650 °C is related to the decomposition of g-C_3N_4 in this region. The horizontal thermal curve observed above at 800 °C corresponds to the metal oxide residue. Thus, Co-g-C_3N_4-imine/TiO_2 can be used as a composite photocatalyst at a relatively high temperature up to 300 °C.

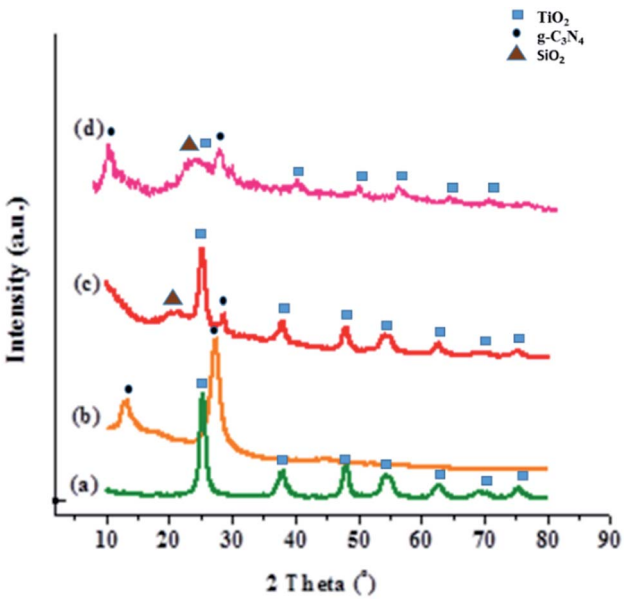

Fig. 3 XRD pattern of (a) TiO_2, (b) g-C_3N_4, (c) g-C_3N_4-imine/TiO_2, and (d) the Co-g-C_3N_4/TiO_2 nanohybrid.

3.2 Catalytic activity

3.2.1 Photo-assisted aerobic oxidation of benzylic alcohols. Initially, the catalytic applicability was explored in the aerobic oxidation of 4-chlorobenzyl alcohol in the presence of NHPI as a model substrate. To access the optimum reaction profile, the effect of various parameters such as the quantity of the catalyst, NHPI amount, solvent, oxidant, and temperature under visible light irradiation were studied for this reaction. The results of the optimization study are presented in Table 1. First, to demonstrate the role of the catalyst and NHPI in the oxidation of 4-chlorobenzyl alcohol, the selected reaction was carried out in their absence, wherein no detectable yields were achieved (Table 1, entries 1 and 2). Indeed, the use of catalysts as well as NHPI for the promotion of the reaction is essential. Further, to explore the effect of the solvent, the test reaction was performed in solvents such as MeCN, EtOAc, H_2O, and EtOH, as well as under solvent-free conditions. Among them, MeCN was recognized as the most favorable solvent (Table 1, entry 7). Then, we attempted different temperatures and 70 °C was preferable (Table 1, entries 7–11). Also, the various dosages of the synthesized catalyst were evaluated and the best result was achieved with 2 mg of the catalyst (Table 1, entry 7, 12 and 13).

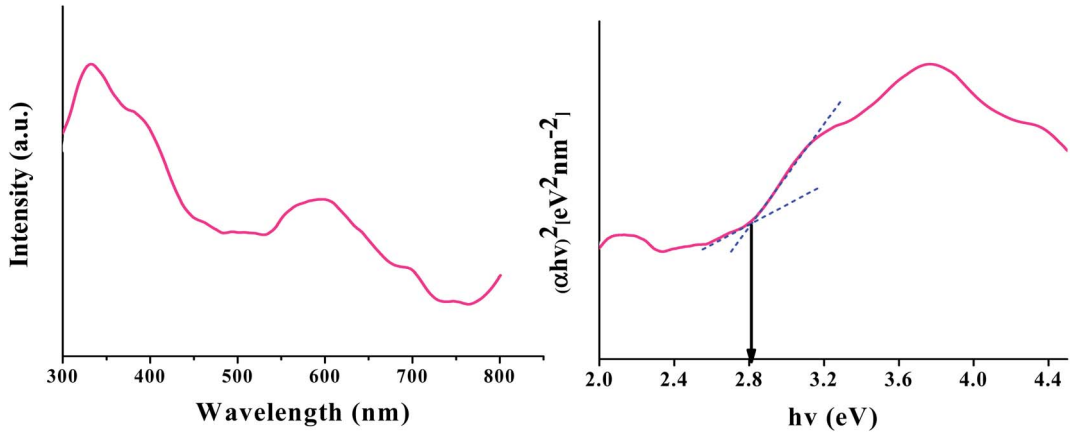

Fig. 4 UV-DR spectra of the Co-C_3N_4-Imine/TiO_2 nanohybrid.

Increasing the amount of the catalyst to more than 3 mg showed no substantial improvement in the yield, whereas the reaction took a long time and was not completed by decreasing the amount of catalyst to 1 mg. The amount of co-catalyst is another variable having a strong influence on the conversion of the desired product. A survey of the results revealed that 0.012 mmol of NHPI is the most effective amount (Table 1, entries 7 and 14). In the next step, to analyze the influence of the oxidant on the reaction progress, common oxidants such as O_2, H_2O_2, TBHP, TBAOX, and Oxon was screened, and the results showed that the air condition was the best choice for completing the reaction (Fig. S4†). Therefore, the optimized reaction conditions were identified as follows: Co-g-C_3N_4-imine/TiO_2 nanohybrid (2 mg 0.5 mol%), NHPI (0.012 mmol), MeCN (0.5 mL) at 70 °C under air and visible light. The ability of TiO_2, g-C_3N_4, $Co(OAc)_2$, g-C_3N_4-imine, and Co-g-C_3N_4-imine/TiO_2 nanohybrid to promote the oxidation of 4-chlorobenzyl alcohol was then evaluated under the selected conditions (Fig. S5†). The first four compounds revealed poor activity under this condition, while the superior catalytic performance of Co-g-C_3N_4-imine/TiO_2 nanohybrid was confirmed.

Table 1 Screening of factors on the aerobic oxidation of 4-chlorobenzyl alcohol under air condition[a]

Entry	Solvent	Temp. (°C)	Catalyst (mg)	NHPI (mg)	Yield[b] (%)
1	MeCN	70	—	2	—
2	MeCN	70	2	—	—
3	S. F.	70	2	2	40
4	H_2O	70	2	2	10
5	EtOH	70	2	2	20
6	EtOAc	70	2	2	85
7	**MeCN**	**70**	**2**	**2**	98
8	MeCN	60	2	2	80
9	MeCN	50	2	2	62
10	MeCN	40	2	2	50
11	MeCN	25	2	2	45
12	MeCN	70	1	2	55
13	MeCN	70	3	2	95
14	MeCN	70	2	1	57

[a] Reactions were run for 1.5 h under air in 0.5 mL solvent containing 0.125 mmol 4-chlorobenzyl alcohols in visible light (CFL, 40 W). [b] GC Yield.

To explore the generality and scope of the oxidation reaction and the effect of the Co-g-C_3N_4-imine/TiO_2 catalytic system, the oxidation of various benzylic alcohols was investigated under optimized conditions. As shown in Table 2, in all the cases of substituted benzyl alcohols, the reaction could afford the corresponding aldehydes and ketones in good to high yields. In addition, no over-oxidation was recognized; thus, the selectivity of the procedure was dominant. As compared with bare benzyl alcohol, the substrates containing electron-donating groups such as -OMe, -Me, and -CMe_3 seemed to be more favorable for the reaction with a good to high conversion ratio (entries 2, 3 and 5). On the other hand, the benzyl alcohols substituted with electron-withdrawing groups such as $-NO_2$ exhibited a decreased conversion ratio and required a longer reaction time to complete this transformation (entry 8). Secondary benzylic alcohols could also be successfully converted to the corresponding ketones (entries 9–12). To probe the chemoselectivity of the method, 4-methylsulfonyl benzyl alcohol was subjected to an oxidation reaction (entries 13). The results indicated that the sulfide group remained intact and related carbonyl compounds were obtained as sole products. It should be noted that the attempts to oxidize leaner aliphatic alcohols under different conditions failed.

3.2.2 Aerobic photo-assisted synthesis of benzimidazoles using benzyl alcohols. To further continue our study, with the effective exploited aerobic oxidation benzyl alcohols in hand, the photocatalytic performance of the Co-g-C_3N_4-imine/TiO_2 nanohybrid was investigated in the synthesis of benzimidazoles through the oxidative coupling of alcohols with aromatic diamines. First, the reaction of 4-chlorobenzyl alcohol (0.12 mmol) with 1,2-phenylenediamine (0.15 mmol) under air in the presence of NHPI was chosen as a model. The data for the optimization of a model reaction are given in Table 3. The inspection of the results in Table 3 (entries 1–6) revealed that the efficiency of the reaction was dependent on the nature of the solvent. The best performance was achieved in MeCN. The screening temperature effect indicated that with *s* decreasing

Table 2 Aerobic oxidation of benzylic alcohols using NHPI/air oxidative system catalyzed by the Co-g-C_3N_4-imine/TiO_2 nanohybrid[a]

Entry	Alcohol	Product[b]	Time (h)	Yield[c] (%)
1	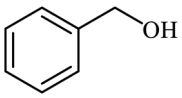	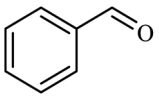	1.5	98
2	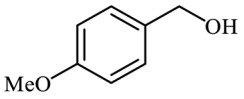	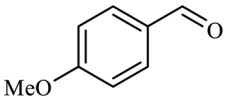	1.6	92
3	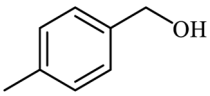	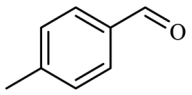	1.6	96
4	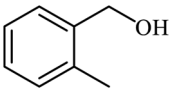	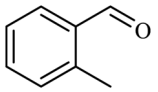	1.8	94
5	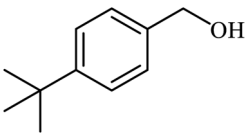	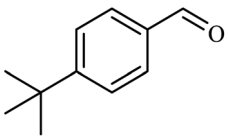	1.8	85
6	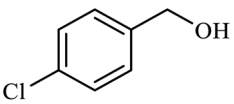	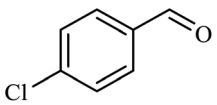	1.5	98
7	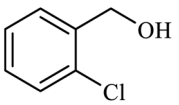	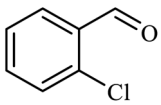	1.8	88
8	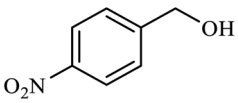	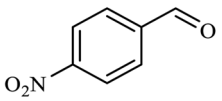	2.5	62
9	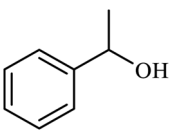	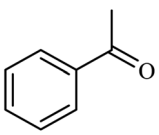	2.5	92
10	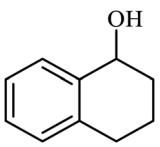	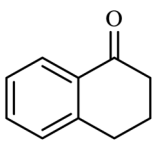	4	67
11	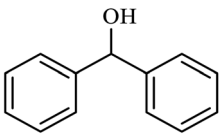	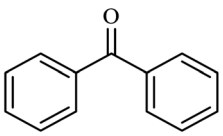	4	71
12	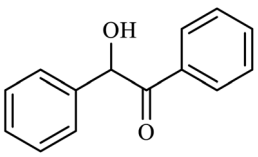	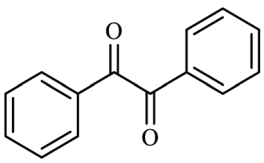	3	82

Table 2 (*Contd.*)

Entry	Alcohol	Product[b]	Time (h)	Yield[c] (%)
13	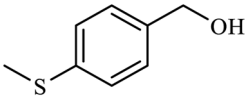	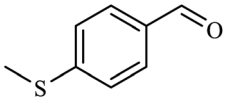	2	95

[a] The reactions were run with substrate (0.125 mmol), NHPI (0.012 mmol), and cat (2 mg) under air at 70 °C in MeCN (0.5 mL), visible light (CFL, 40 W). [b] The products were identified by comparison with authentic sample retention times from GC analysis and NMR spectra. [c] The selectivity of the products was >99% based on GC analysis.

temperature from 70 to 25 °C, the yield was significantly reduced (Table 3, entries 7–10). The effect of the catalyst and NHPI in the model system was studied with a further set of experiments. The result proved that did not proceed in the absence of the catalyst and NHPI. Thus, their use for the promotion of the reaction is crucial (Table 3, entries 13 and 14) (Scheme S2†). Entries 6, 11–12, 15 and 16 in Table 3 show the effect of the catalyst as well as NHPI on the reaction performance by varying the loading amount. The results showed that 3 mg of the catalyst and 0.012 mmol of NHPI were the best choices for completing the reaction. In addition, the reaction was further optimized for the oxidant nature (Table 3, entries 17–19). We also conducted the reaction under O_2 stream as an oxidant and found it less effective than air (70%). Thus, the reaction showed the best efficiency using a molar ratio of 0.12 : 0.15 : 0.012 for benzyl alcohol/diamine/NHPI with 3 mg of catalyst in MeCN (0.5 mL) at 70 °C under air and visible light.

To establish the general applicability of the method, various benzylic alcohols were subjected to the condensation of 1,2-phenylenediamines to produce benzimidazole derivatives using a catalytic amount of Co-g-C_3N_4-imine/TiO_2 (Table 4). The results revealed that the reaction rate was affected by the electronic nature of the substrates. Benzyl alcohols bearing electron-releasing groups were converted to the benzimidazole derivatives as a good substrate (Table 4, entries 2, 5, and 7). Nevertheless, both benzylic alcohol and diamine molecules with a strong electron-withdrawing group such as the nitro group on the phenyl ring are significantly inactive in this catalytic system (Table 4, entry 4 and 10).

3.2.3 Aerobic photo-assisted synthesis of benzimidazoles using benzaldehydes. Next, the possibility of benzimidazole synthesis *via* the reaction of 1,2-phenylenediamine and benzaldehydes as starting materials under the catalytic influence of the Co-g-C_3N_4-imine/TiO_2 nanohybrid was tested. To achieve new reaction conditions, different factors were screened. According to the data summarized in Table S1,† the reaction of 4-chlorobenzaldehyde (0.12 mmol) with 1,2-phenylenediamine (0.15 mmol) in ethanol (0.5 mL) containing 2 mg of the Co-g-C_3N_4-

Table 3 Screening of factors in the synthesis of benzimidazole by the reaction of 4-chlorobenzyl alcohol and 1,2-phenylenediamine catalyzed by the Co-g-C_3N_4-imine/TiO_2 nanohybrid[a]

Entry	Solvent	Temp. (°C)	Catalyst (mg)	NHPI (mmol)	Yield[b] (%)
1	Solvent free	70	3	0.012	20
2	H_2O	70	3	0.012	—
3	HOAc	70	3	0.012	—
4	EtOH	70	3	0.012	5
5	EtOAc	70	3	0.012	75
6	**MeCN**	**70**	**3**	**0.012**	**90**
7	MeCN	60	3	0.012	73
8	MeCN	50	3	0.012	45
9	MeCN	40	3	0.012	42
10	MeCN	25	3	0.012	32
11	MeCN	70	2	0.012	81
12	MeCN	70	1	0.012	65
13	MeCN	70	—	0.012	—
14	MeCN	70	3	—	—
15	MeCN	70	3	0.006	72
16	MeCN	70	3	0.018	81
17[c]	MeCN	70	3	0.012	—
18[d]	MeCN	70	3	0.012	—
19[e]	MeCN	70	3	0.012	72

[a] Reactions were run for 4 h in 0.5 mL of the solvent containing 0.12 mmol 4-chlorobenzyl alcohols, 0.15 mmol 1,2-phenylenediamine, 0.012 mmol NHPI in visible light (CFL, 40 W), air condition. [b] GC Yield. [c] H_2O_2, and TBHP as oxidant. [d] H_2O_2, and TBHP as oxidant. [e] O_2 stream.

Table 4 Synthesis of benzimidazole derivatives from benzyl alcohols and 1,2-phenylenediamines[a]

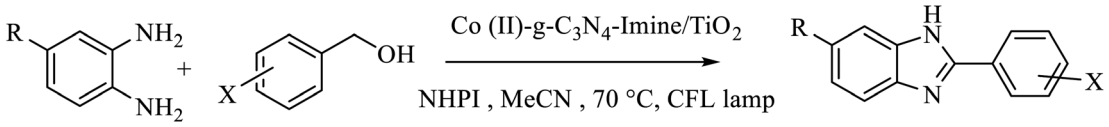

Entry	Diamine, R	Alcohol, X	Product[b]	Time (h)	Yield[c] (%)
1	H	H	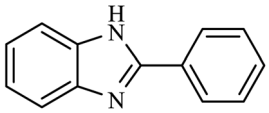	4	92
2	H	4-Cl	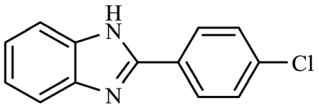	4	90
3	H	2-Cl	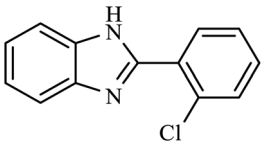	4	75
4	H	4-NO_2	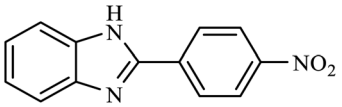	6	—
5	H	4-OMe	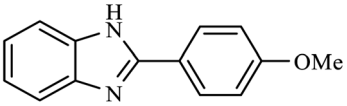	4.5	88
6	H	4-SMe	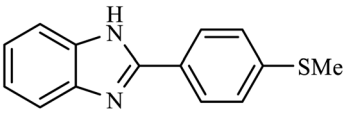	4.5	35
7	H	4-Me	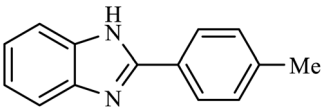	4.5	82
8	H	2-Me	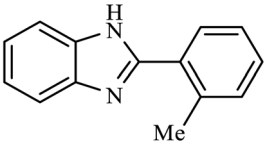	4.5	73
9	H	4-*t*-Bu	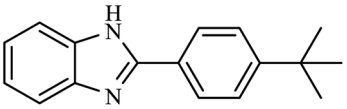	4.5	73
10	NO_2	4-Me	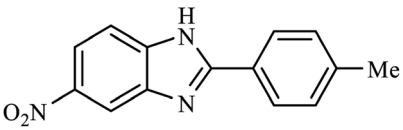	6	—
11	Me	4-Me	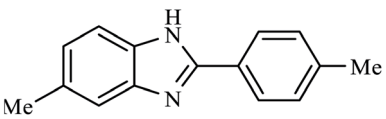	4.5	62

[a] Reaction conditions: benzyl alcohol (0.12 mmol), 1,2-phenylene diamine (0.15 mmol), catalyst (3 mg), NHPI (0.012 mmol) in 0.5 mL MeCN at 70 °C under air and visible light (CFL. 40 W). [b] The products were identified by ^{1}H NMR spectroscopy. [c] Isolated yield.

imine/TiO_2 nanohybrid proceeded quantitatively within 50 min under aerobic conditions at 60 °C with no need for NHPI. As a result, we then focused on the evaluation of the substrate scope for the synthesis of benzimidazoles. Various aryl aldehydes were allowed to react with 1,2-phenylenediamines. The corresponding benzimidazoles were produced in high yields, except for the

Table 5 Synthesis of benzimidazole derivatives from benzaldehydes and 1,2-phenylenediamines[a]

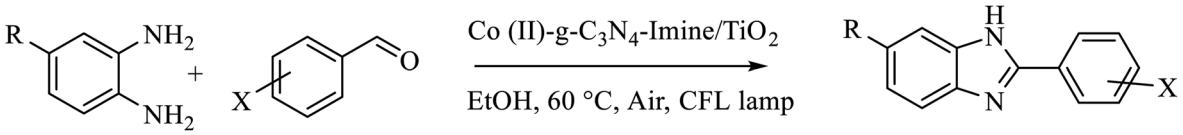

Entry	Diamine, R	Alcohol, X	Product[b]	Time (min)	Yield[c] (%)
1	H	H	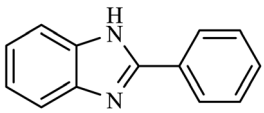	45	98
2	H	4-Cl	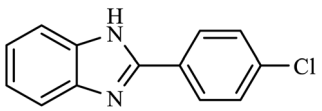	50	97
3	H	2-Cl	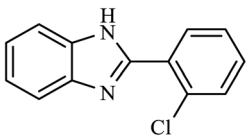	60	95
4	H	4-NO_2	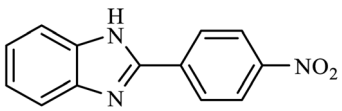	120	35
5	H	2-NO_2	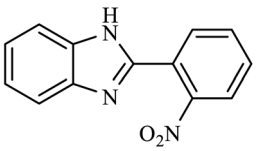	140	30
6	H	4-OMe	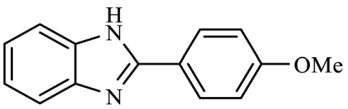	65	96
7	H	4-OH	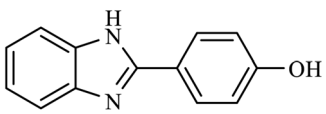	90	50
8	H	4-Me	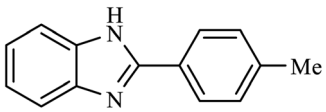	60	95
9	NO_2	H	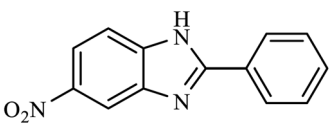	130	20
10	Me	H	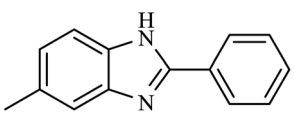	55	90

[a] Reaction conditions: benzaldehyde (0.12 mmol), 1,2-phenylenediamine (0.15 mmol), catalyst (2 mg), in 0.5 mL EtOH at 60 °C under air, visible light (CFL. 40 W). [b] The products were identified by ^{1}H NMR spectroscopy. [c] Isolated yield.

electron-deficient ones, which induced a negative influence on the reaction efficiency in this catalytic system and formed in moderate yields (Table 5, entries 4, 5 and 9).

3.3 Photocatalytic activity

To investigate the photocatalytic activity of the Co-g-C_3N_4-imine/TiO_2 nanohybrid on the aerobic oxidation of benzyl alcohols and synthesis of benzimidazoles, we compared the photocatalytic activity of the Co-g-C_3N_4-imine/TiO_2 nanohybrid with that of other nanooxometals such as γ-Fe_2O_3, g-C_3N_4, and TiO_2 and their material precursors such as g-C_3N_4/TiO_2, Co-C_3N_4/TiO_2, Co-g-C_3N_4-imine, and Co-g-C_3N_4-imine/Fe_2O_3 in the aerobic oxidation and oxidative coupling model systems under the same conditions; the results are depicted in Fig. 5.

Indeed, with the replacement of TiO_2 with another metal oxide such as Fe_2O_3, a significant reduction in the product yields was observed in the oxidative systems and indicated the core dependence of the catalytic activity. Thus, the photocatalytic activity depends greatly on the TiO_2 core and affected the catalytic performance of the Co-g-C_3N_4-imine/TiO_2 nanohybrid.

Then, we tried to utilize the relative contributions of light and thermal processes in the conversion efficiencies. In this line, the contributions of light irradiation to the conversion efficiency were evaluated by subtracting the conversion of the reaction in the dark (thermal effect) from the overall conversion observed when the system was irradiated under identical reaction conditions.

When the light sources were UV light, LED, sun light, Actinic BL lamp, and CFL lamps (compact fluorescent lamp, $\lambda = 400$–700 nm, 40 W), the light contributions for oxidation reactions of 4-chlorobenzyl alcohol and synthesis of benzimidazole were investigated (Fig. 6a and b). We can see that CFL light gave a greater contribution to irradiation to the overall conversion rate in both the reactions. The results endorsed light dependence, which is due to the photocatalytic effect of the TiO_2 core and g-C_3N_4 on the efficiency of the Co-g-C_3N_4-imine/TiO_2 for these reaction systems.

Further, we explored the relative contribution of thermal and photochemical processes to the oxidative reactions. To achieve this goal, the aerobic oxidation of 4-chlorobenzyl alcohol and synthesis of benzimidazoles from 4-chlorobenzyl alcohol were conducted under dark as well as different wavelength ranges of irradiation (Fig. 6c, 6c′, 6d and 6d′). Further, the above-mentioned wavelength ranges are provided through a series of optical low-pass filters with the ability to block light below a specific cut-off wavelength (see ESI†). Subtracting the conversion in the dark from the overall conversion under light gave a contribution of light to the conversion efficiency. For example, for the aerobic oxidation of 4-chlorobenzyl alcohols, without any filters, the irradiation of light with wavelengths ranging from 400 to 800 nm gives a 4-chlorobenzaldehyde yield of 98%. The yield declines to 72%, 60%, and 40% when the wavelength range of the irradiation is 450–800, 550–800, and 600–800 nm, respectively. The contribution of 400–450 nm light accounts for about 35% ((73 − 47)/73 × 100%) in the total light-induced yield. Also, the light in the wavelength range of 450–550, 550–600, and 600–800 nm accounts for 16%, 27%, and 20% of the light-induced yield, respectively (Fig. 6c). Moreover, a similar trend was obtained for the oxidative system of benzimidazoles from 4-chlorobenzyl alcohols with 90%, 66%, 51%, and 30% yield relative to the mentioned wavelength ranges, the result is depicted clearly in Fig. 6d.

Finally, to confirm the light dependency of the photocatalyst, the action spectrum was also examined. The action spectra show the one-to-one mapping between the wavelength-dependent photocatalytic rate and the light extinction spectrum. In this regard, the reaction rates of the oxidation of 4-chlorobenzyl alcohol and the synthesis of 2-[4-chlorophenyl]-benzimidazole using Co-g-C_3N_4-imine/TiO_2 under irradiation with different wavelengths were investigated. A good accordance between the apparent quantum yield (AQY) with the diffuse reflectance spectrum of the Co-g-C_3N_4-imine/TiO_2 nanohybrid was observed in both the oxidative reaction systems (Fig. 7). These results convinced us that the reactions are performed in a photocatalytic manner.

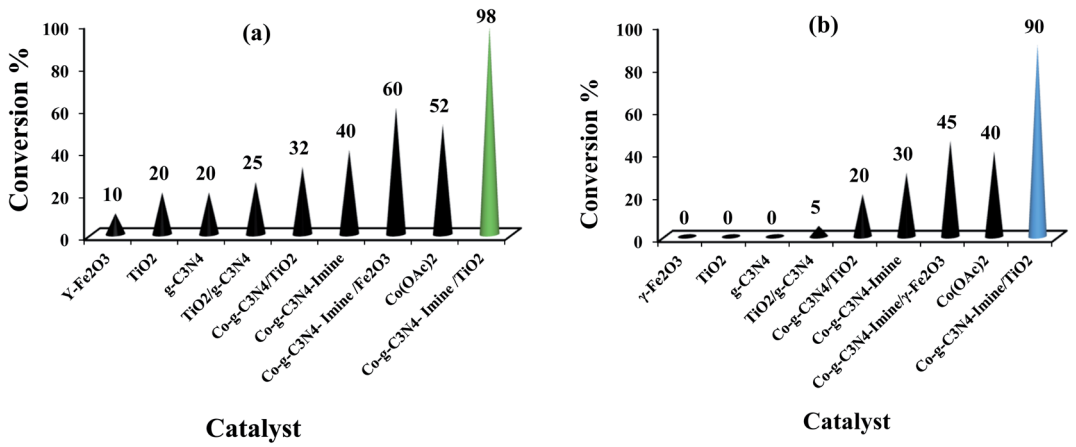

Fig. 5 Comparison of the catalytic activity of Co-g-C_3N_4-imine/TiO_2 with parent materials in (a) the aerobic oxidation of 4-chlorobenzyl alcohol. (b) One-pot aerobic synthesis of benzimidazole under the optimization conditions from 4-chlorobenzyl alcohol and 1,2-phenylenediamine.

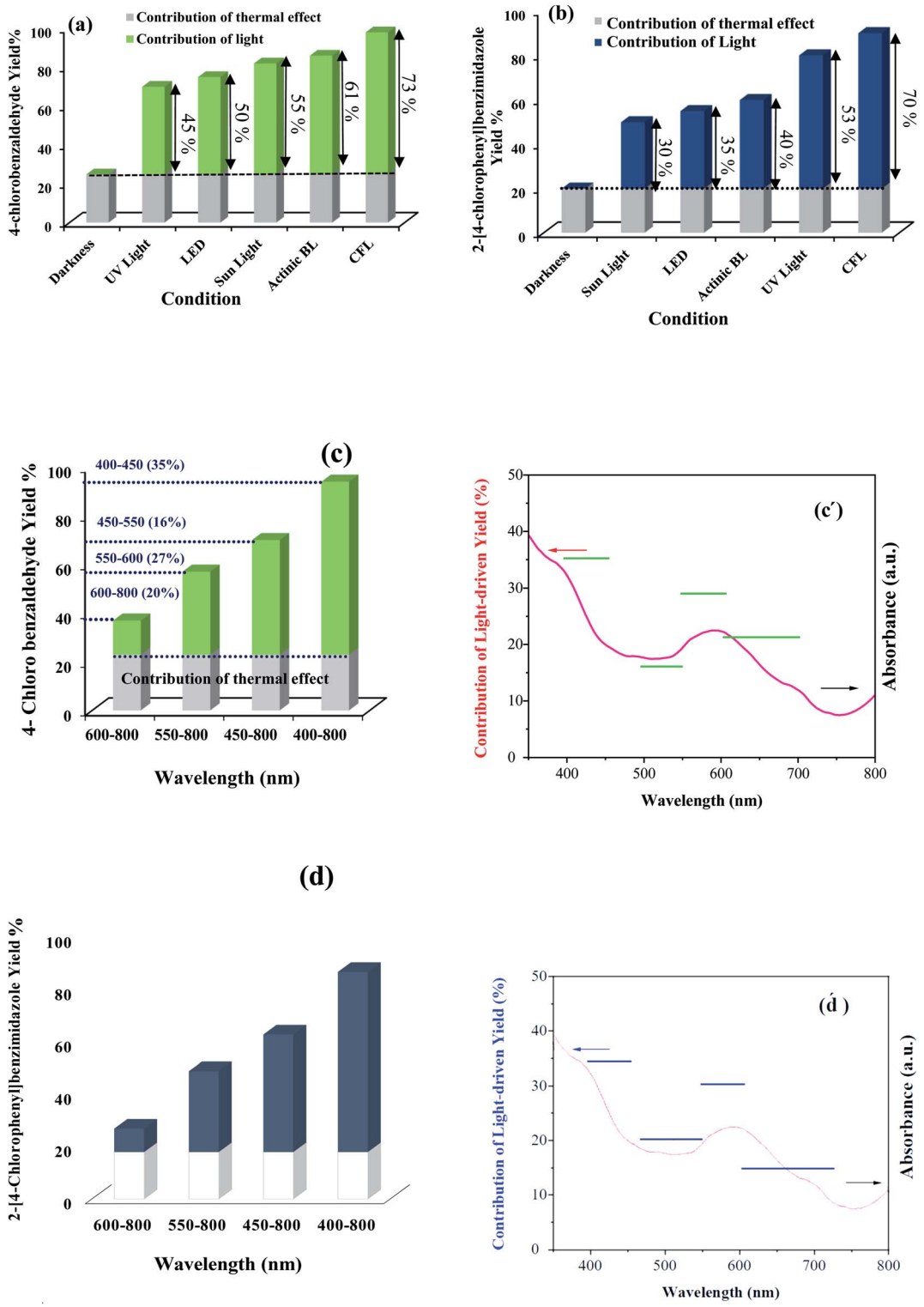

Fig. 6 Dependence of the catalytic activity of Co-g-C_3N_4-imine/TiO_2 for (a) the oxidation of 4-chlorobenzyl alcohol. (b) Synthesis of 2-[4-chlorophenyl]-benzimidazole on the irradiation wavelength. (c) Dependence of 4-chlorobenzaldehyde yield on the irradiation wavelength and the action spectrum of the photocatalytic reaction, in which the light-driven conversion is plotted against the irradiation wavelength. (d) Dependence of 2-[4-chlorophenyl]-benzimidazole yield on the irradiation wavelength and the action spectrum of the photocatalytic reaction, in which the light-driven conversion is plotted against the irradiation wavelength.

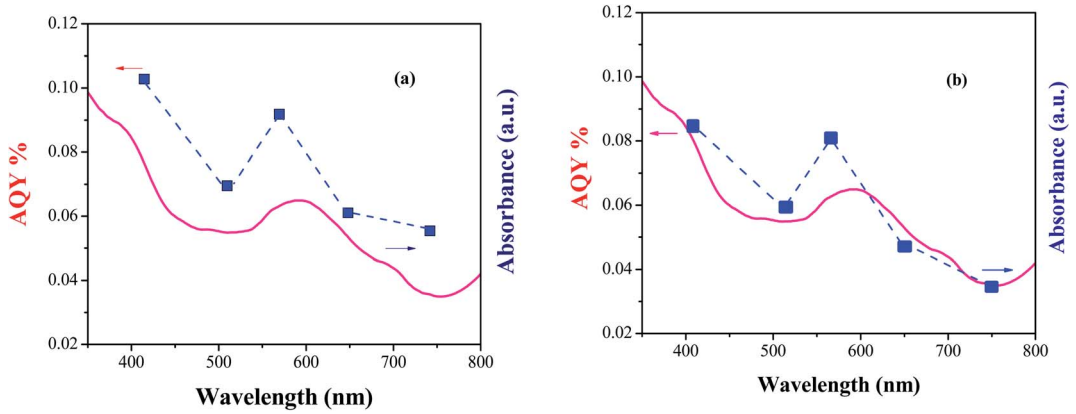

Fig. 7 Action spectrum for (a) the oxidation of 4-chlorobenzyl alcohol and (b) synthesis of 2-[4-chlorophenyl] benzimidazole from 4-chlorobenzyl alcohol and 1,2-phenylenediamine using the Co-g-C_3N_4-imine/TiO_2 photocatalyst under the optimized reaction condition. The AQY *versus* the respective wavelengths of the reaction is plotted. AQY was calculated with the following equation: AQY (%) = [(Y_{vis} − Y_{dark}) × 2/(photons that entered into the reaction vessel)] × 100, where Y_{light} and Y_{dark} are the amounts of products formed under light irradiation and dark conditions, respectively.

Table 6 Comparison of the catalytic activity of Co-g-C_3N_4-imine/TiO_2 with that of other previously reported catalysts for the oxidation of alcohols using 4-chlorobenzyl alcohol

Entry	Catalyst	Catalyst (mg)	Conditions	Time (h)	Yield (%)	Ref.
1	Co-g-C_3N_4-imine/TiO_2	2 mg	70 °C, MeCN, NHPI, air, visible light (CFL lamp)	1.5	98	This work
2	Fe(acac)$_3$/g-C_3N_4	25 mg	r.t, MeCN, LED λ >400 nm	5	84	52
3	CNNA[a]	20 mg	70 °C, MeCN, O_2, sunlight	9	61.4	53
4	AR[b]/TiO_2	4 mg	r.t, BTF[c], TEMPO, visible-light, toluene, O_2	15	59	54
5	mp[d]g-C_3N_4	50 mg	100 °C, trifluorotoluene, O_2, visible light	3	79	55
6	Co-NG[e]-750	5 mg	120 °C, DMF, O_2	5	84.2	56
7	TiO_2	50 mg	r.t, O_2, LED lamp	4	>99	57
8	10CN[f]-0.5Si-WO	20 mg	r.t, MeCN, O2, 300 W Xe lamp	3	76.8	58
9	$Pt_{0.8}Cu_{0.2}$/anatase	5 mg	25 °C, toluene, O_2, visible light	4	73	59
10	Mpg-CN[g]	50 mg	100 °C, pH 0 (1 m HCl), O_2, visible light	2	46	60

[a] Nitric acid-pretreated melamine precursor. [b] Alizarin Red. [c] Benzotrifluoride. [d] Mesoporous carbon nitride. [e] Nitrogen-doped graphene. [f] g-C_3N_4 nanosheets. [g] Mesoporous graphitic carbon nitride.

3.4 Stability and reusability of the catalyst

The stability and reusability of the catalyst are very important parameters for any research applied in terms of environmental conservation and cost. In this context, the feasibility of reusing the catalyst was also studied for the aerobic oxidation of 4-chlorobenzyl alcohol as a model reaction. After completing the reaction, the catalyst was separated by the centrifugation and

Table 7 Comparison of catalytic activity of Co-g-C_3N_4-imine/TiO_2 with that of other previously reported catalysts for the synthesis of benzimidazole using 4-chlorobenzyl alcohol and 1,2-phenylenediamine

Entry	Catalyst	Catalyst (mg)	Conditions	Time (h)	Yield (%)	Ref.
1	Co-g-C_3N_4-imine/TiO_2	3 mg	70 °C, MeCN, NHPI, air, visible light (CFL lamp)	4	90	This work
2	[Ir(cod)2,6-DiAmPy(iPr)$_2$]	1.4 mol%	110 °C, KO^{t}Bu, diglyme	24	68	61
3	Co-PNNH[a]	5 mol%	150 °C, $NaHBEt_3$, toluene	24	55	46
4	Pt@TiO_2	5 mg	30 °C, $h\nu$ (λ > 300 nm), N_2, MeCN	12	82	62
5	MoO_3–SiO_2	20 wt%	70 °C, H_2O_2	7	86	63
6	TiO_2@PMHSIPN[b]	2 mol%	160 °C, S.F, K_2CO_3	12	84	64
7	[RuCl(L1)[c](CH_3CN)$_2$]Cl	0.25 mol%	165 °C, dppe[d], $NaBPh_4$	12	96	65
8	CuCl	5 mol%	r.t, S.F, bpy, TEMPO	12	91	66
9	Co_3O_4@Al_2O_3/SiO_2	5 mol%	120 °C, air, O_2	6	82	67

[a] (pyridine-based PNNH pincer). [b] polymethylhydrosiloxane (PMHS). [c] L1 = 2,6-bis(1H-imidazole-2-yl)pyridine. [d] 1,2-bis(diphenylphosphanyl) ethane.

decantation of the reaction mixture, dried in a vacuum oven at 40 °C, and then reused. Though the aerobic oxidation proceeded well using the recovered heterogeneous catalyst, no catalytic activity was observed in the filtrate solution. Also, to screen the heterogeneous nature of the catalyst, a leaching test was conducted for the aerobic oxidation of 4-chlorobenzyl alcohol under the optimized reaction condition. For this reason, in the middle of the reaction time, the catalyst was completely collected using centrifugation and the reaction was allowed to continue under the same conditions. The reaction did not proceed further even after 1 h (followed by TLC). These results indicate the heterogeneous property of the prepared catalyst. Further, the amount of cobalt leaching was also determined in the fresh and the reused catalyst by ICP-OES analysis, and no leaching of cobalt was observed. Based on these observations, the catalyst is stable under the reaction conditions and can be recovered and reused (Fig. S6†).

The comparison of the FT-IR spectrum of the used Co-g-C_3N_4-imine/TiO_2 nanocatalyst (Fig. S7†) with that of a fresh one affirms that the structure of the catalyst remains almost intact after five runs of recovery. Similar to the abovementioned procedures, the test for catalyst reusability were performed for the oxidative coupling of 4-chlorobenzyl alcohol (or 4-chlorobenzaldahyde) with 1,2-phenylenediamine to produce benzimidazole.

Tables 6 and 7 show the merit of these operation protocols in comparison with the previously Co and TiO_2/C_3N_4-based catalytic methods in the aerobic oxidation of benzyl alcohol and synthesis of benzimidazole from benzyl alcohol as a model substrate. These comparisons revealed that the presented catalytic oxidation systems are attractive from the point of view of catalyst loading, reaction time, yield, and especially, reaction conditions.

4 Conclusion

In summary, we introduced a novel and photoefficient nanocatalyst consisting of cobalt incorporated in the g-C_3N_4-imine/TiO_2 nanohybrid as a heterojunction photocatalyst. This catalyst system promoted several different transformations in a one-pot reaction: the aerobic oxidation of benzyl alcohols and subsequently the dehydrogenative coupling of primary benzylic alcohols and aryl diamines for the direct synthesis of benzimidazoles with good to high yields. The protocol is also capable of oxidative coupling of benzaldehydes with the aryl diamines producing benzimidazoles. This new heterogeneous nanocatalyst improved the photocatalytic activity predominantly due to the synergistic effects of Co-carbon nitride on TiO_2 nanoparticles. High chemical and thermal stability, avoiding expensive starting materials, using air as an ideal oxidant and visible light as a safe energy source, excellent durability, convenient reusability of catalyst, and mild reaction conditions are the advantages of this catalytic process, which make it a potential candidate for addressing many of the challenges of green chemistry. Thus, our study could provide an impressive strategy for various photocatalytic applications under safe and practically attainable conditions.

Conflicts of interest

There are no conflicts to declare.

Acknowledgements

Support for this work by the Research Council of the University of Birjand is highly appreciated. Dr Narges Pourmorteza was supported by a grant from Basic Sciences Research Fund (no. BSRF-chem-399-02).

References

1 R. A. Sheldon and J. M. Woodley, Role of biocatalysis in sustainable chemistry, *Chem. Rev.*, 2018, **118**(2), 801–838.
2 Q. Wang, T. Hisatomi, Q. Jia, H. Tokudome, M. Zhong, C. Wang, Z. Pan, T. Takata, M. Nakabayashi, N. Shibata, *et al.*, Scalable water splitting on particulate photocatalyst sheets with a solar-to-hydrogen energy conversion efficiency exceeding 1%, *Nat. Mater.*, 2016, **15**(6), 611–615.
3 D. M. Schultz and T. P. Yoon, Solar synthesis: prospects in visible light photocatalysis, *Science*, 2014, **343**, 6174.
4 N. Corrigan, S. Shanmugam, J. Xu and C. Boyer, Photocatalysis in organic and polymer synthesis, *Chem. Soc. Rev.*, 2016, **45**(22), 6165–6212.
5 S. N. R. Inturi, M. Suidan and P. G. Smirniotis, Influence of synthesis method on leaching of the Cr-TiO_2 catalyst for visible light liquid phase photocatalysis and their stability, *Appl. Catal., B*, 2016, **180**, 351–361.
6 M. Anpo and P. V. Kamat, *Environmentally benign photocatalysts: applications of titanium oxide-based materials*, Springer Science & Business Media, 2010.
7 M. Qamar, Q. Drmosh, M. I. Ahmed, M. Qamaruddin and Z. H. Yamani, Enhanced photoelectrochemical and photocatalytic activity of WO_3-surface modified TiO_2 thin film, *Nanoscale Res. Lett.*, 2015, **10**(1), 1–6.
8 Y.-C. Pu, G. Wang, K.-D. Chang, Y. Ling, Y.-K. Lin, B. C. Fitzmorris, C.-M. Liu, X. Lu, Y. Tong, J. Z. Zhang, *et al.*, Au nanostructure-decorated TiO_2 nanowires exhibiting photoactivity across entire UV-visible region for photoelectrochemical water splitting, *Nano Lett.*, 2013, **13**(8), 3817–3823.
9 S. A. Ansari, M. M. Khan, M. O. Ansari and M. H. Cho, Silver nanoparticles and defect-induced visible light photocatalytic and photoelectrochemical performance of Ag@m-TiO_2 nanocomposite, *Sol. Energy Mater. Sol. Cells*, 2015, **141**, 162–170.
10 V. Subramanian, E. Wolf and P. V. Kamat, Semiconductor-metal composite nanostructures. To what extent do metal nanoparticles improve the photocatalytic activity of TiO_2 films?, *J. Phys. Chem. B*, 2001, **105**(46), 11439–11446.
11 W.-J. Ong, L.-L. Tan, Y. H. Ng, S.-T. Yong and S.-P. Chai, Graphitic carbon nitride (g-C_3N_4)-based photocatalysts for artificial photosynthesis and environmental remediation: are we a step closer to achieving sustainability?, *Chem. Rev.*, 2016, **116**(12), 7159–7329.

12 J. Wen, J. Xie, X. Chen and X. Li, A review on g-C_3N_4-based photocatalysts, *Appl. Surf. Sci.*, 2017, **391**, 72–123.
13 Y. Wang, X. Wang and M. Antonietti, Polymeric graphitic carbon nitride as a heterogeneous organocatalyst: from photochemistry to multipurpose catalysis to sustainable chemistry, *Angew. Chem., Int. Ed.*, 2012, **51**(1), 68–89.
14 V. W. Lau, I. Moudrakovski, T. Botari, S. Weinberger, M. B. Mesch, V. Duppel, J. Senker, V. Blum and B. V. Lotsch, Rational design of carbon nitride photocatalysts by identification of cyanamide defects as catalytically relevant sites, *Nat. Commun.*, 2016, **7**(1), 1–10.
15 S. Cao, J. Low, J. Yu and M. Jaroniec, Polymeric photocatalysts based on graphitic carbon nitride, *Adv. Mater.*, 2015, **27**(13), 2150–2176.
16 X. Guo, C. Hao, G. Jin, H.-Y. Zhu and X.-Y. Guo, Copper nanoparticles on graphene support: an efficient photocatalyst for coupling of nitroaromatics in visible light, *Angew. Chem., Int. Ed.*, 2014, **53**(7), 1973–1977.
17 J. Xu, G. Wang, J. Fan, B. Liu, S. Cao and J. Yu, g-C3N4 modified TiO_2 nanosheets with enhanced photoelectric conversion efficiency in dye-sensitized solar cells, *J. Power Sources*, 2015, **274**, 77–84.
18 M. Caux, F. Fina, J. T. S. Irvine, H. Idriss and R. Howe, Impact of the annealing temperature on Pt/g-C_3N_4 structure, activity and selectivity between photodegradation and water splitting, *Catal. Today*, 2017, **287**, 182–188.
19 Q. Tay, P. Kanhere, C. F. Ng, S. Chen, S. Chakraborty, A. C. H. Huan, T. C. Sum, R. Ahuja and Z. Chen, Defect engineered g-C_3N_4 for efficient visible light photocatalytic hydrogen production, *Chem. Mater.*, 2015, **27**(14), 4930–4933.
20 X. Wang, S. Blechert and M. Antonietti, Polymeric graphitic carbon nitride for heterogeneous photocatalysis, *ACS Catal.*, 2012, **2**(8), 1596–1606.
21 X. Zhong, M. Jin, H. Dong, L. Liu, L. Wang, H. Yu, S. Leng, G. Zhuang, X. Li and J. Wang, TiO_2 nanobelts with a uniform coating of g-C_3N_4 as a highly effective heterostructure for enhanced photocatalytic activities, *J. Solid State Chem.*, 2014, **220**, 54–59.
22 G. Liao, S. Chen, X. Quan, H. Yu and H. Zhao, Graphene oxide modified g-C_3N_4 hybrid with enhanced photocatalytic capability under visible light irradiation, *J. Mater. Chem.*, 2012, **22**(6), 2721–2726.
23 Y. Wang, R. Shi, J. Lin and Y. Zhu, Enhancement of photocurrent and photocatalytic activity of ZnO hybridized with graphite-like C_3N_4, *Energy Environ. Sci.*, 2011, **4**(8), 2922–2929.
24 X. Wang, X. Chen, A. Thomas, X. Fu and M. Antonietti, Metal-containing carbon nitride compounds: a new functional organic-metal hybrid material, *Adv. Mater.*, 2009, **21**(16), 1609–1612.
25 Z. Ding, X. Chen, M. Antonietti and X. Wang, Synthesis of transition metal-modified carbon nitride polymers for selective hydrocarbon oxidation, *ChemSusChem*, 2011, **4**(2), 274–281.
26 Y. Zhang, A. Thomas, M. Antonietti and X. Wang, Activation of carbon nitride solids by protonation: morphology changes, enhanced ionic conductivity, and photoconduction experiments, *J. Am. Chem. Soc.*, 2009, **131**(1), 50–51.
27 S. C. Yan, S. B. Lv, Z. S. Li and Z. G. Zou, Organic-inorganic composite photocatalyst of g-C_3N_4 and TaON with improved visible light photocatalytic activities, *Dalton Trans.*, 2010, **39**(6), 1488–1491.
28 J. Yan, H. Wu, H. Chen, Y. Zhang, F. Zhang and S. F. Liu, Fabrication of TiO_2/C_3N_4 heterostructure for enhanced photocatalytic Z-scheme overall water splitting, *Appl. Catal., B*, 2016, **191**, 130–137.
29 Z. Zhang, D. Jiang, D. Li, M. He and M. Chen, Construction of $SnNb_2O_6$ nanosheet/g-C3N4 nanosheet two-dimensional heterostructures with improved photocatalytic activity: synergistic effect and mechanism insight, *Appl. Catal., B*, 2016, **183**, 113–123.
30 B. Chai, T. Peng, J. Mao, K. Li and L. Zan, Graphitic carbon nitride (g-C_3N_4)-Pt-TiO_2 nanocomposite as an efficient photocatalyst for hydrogen production under visible light irradiation, *Phys. Chem. Chem. Phys.*, 2012, **14**(48), 16745–16752.
31 L. Zhou, L. Wang, J. Zhang, J. Lei and Y. Liu, The preparation, and applications of g-C_3N_4/TiO_2 heterojunction catalysts-a review, *Res. Chem. Intermed.*, 2017, **43**(4), 2081–2101.
32 K. Li, B. Peng, J. Jin, L. Zan and T. Peng, Carbon nitride nanodots decorated brookite TiO_2 quasi nanocubes for enhanced activity and selectivity of visible-light-driven CO_2 reduction, *Appl. Catal., B*, 2017, **203**, 910–916.
33 Y. Zhao, L. Xu, S. Huang, J. Bao, J. Qiu, J. Lian, L. Xu, Y. Huang, Y. Xu and H. Li, Facile preparation of TiO_2/C_3N_4 hybrid materials with enhanced capacitive properties for high performance supercapacitors, *J. Alloys Compd.*, 2017, **702**, 178–185.
34 M. Fu, J. Liao, F. Dong, H. Li and H. Liu, Growth of g-C_3N_4 layer on commercial TiO_2 for enhanced visible light photocatalytic activity, *J. Nanomater.*, 2014, **2014**, 869094.
35 Q. Zhang, H. Wang, Z. Li, C. Geng and J. Leng, Metal-free photocatalyst with visible-light-driven post-illumination catalytic memory, *ACS Appl. Mater. Interfaces*, 2017, **9**(26), 21738–21746.
36 M. Sakar, C.-C. Nguyen, M.-H. Vu and T.-O. Do, Materials and mechanisms of photo-assisted chemical reactions under light and dark conditions: can day-night photocatalysis be achieved?, *ChemSusChem*, 2018, **11**(5), 809–820.
37 Z. Duan, L. Zhang, W. Zhang, L. Lu, L. Zeng, R. Shi and A. Lei, Palladium-Catalyzed Electro-oxidative C-H Amination toward the Synthesis of Pyrido [1, 2-a] benzimidazoles with Hydrogen Evolution, *ACS Catal.*, 2020, **10**(6), 3828–3831.
38 F. Feizpour, M. Jafarpour and A. Rezaeifard, A Tandem Aerobic Photocatalytic Synthesis of Benzimidazoles by Cobalt Ascorbic Acid Complex Coated on TiO_2 Nanoparticles Under Visible Light, *Catal. Lett.*, 2018, **148**(1), 30–40.
39 A. Eskandari, M. Jafarpour, A. Rezaeifard and M. Salimi, A dendritic TiO_2-Co (ii) nanocomposite based on the

melamine catalyzed one-pot aerobic photocatalytic synthesis of benzimidazoles, *New J. Chem.*, 2018, **42**(8), 6449–6456.

40 S. Das, S. Mallick and S. De Sarkar, Cobalt-catalyzed sustainable synthesis of benzimidazoles by redox-economical coupling of o-nitroanilines and alcohols, *J. Org. Chem.*, 2019, **84**(18), 12111–12119.

41 S. Shee, D. Panja and S. Kundu, Nickel-Catalyzed Direct Synthesis of Quinoxalines from 2-Nitroanilines and Vicinal Diols: Identifying Nature of the Active Catalyst, *J. Org. Chem.*, 2020, **85**(4), 2775–2784.

42 A. K. Kabi, R. Gujjarappa, A. Roy, A. Sahoo, D. Musib, N. Vodnala, V. Singh and C. C. Malakar, Transition-Metal-Free Transfer Hydrogenative Cascade Reaction of Nitroarenes with Amines/Alcohols: Redox-Economical Access to Benzimidazoles, *J. Org. Chem.*, 2021, **86**(21), 14597–14607.

43 A. Bera, M. Sk, K. Singh and D. Banerjee, Nickel-catalysed dehydrogenative coupling of aromatic diamines with alcohols: selective synthesis of substituted benzimidazoles and quinoxalines, *Chem. Commun.*, 2019, **55**(42), 5958–5961.

44 M. Zuo, W. Guo, Y. Pang, R. Guo, C. Hou, S. Sun, H. Wu, Z. Sun and W. Chu, Direct synthesis of 2-substituted benzimidazoles via dehydrogenative coupling of aromatic-diamine and primary alcohol catalyzed by a Co complex, *New J. Chem.*, 2020, **44**(34), 14490–14495.

45 R. R. Putta, S. Chun, S. H. Choi, S. B. Lee, D.-C. Oh and S. Hong, Iron (0)-Catalyzed Transfer Hydrogenative Condensation of Nitroarenes with Alcohols: A Straightforward Approach to Benzoxazoles, Benzothiazoles, and Benzimidazoles, *J. Org. Chem.*, 2020, **85**(23), 15396–15405.

46 P. Daw, Y. Ben-David and D. Milstein, Direct synthesis of benzimidazoles by dehydrogenative coupling of aromatic diamines and alcohols catalyzed by cobalt, *ACS Catal.*, 2017, **7**(11), 7456–7460.

47 M. Jafarpour, F. Feizpour, A. Rezaeifard, N. Pourmorteza and B. Breit, Tandem Photocatalysis Protocol for Hydrogen Generation/Olefin Hydrogenation Using Pd-g-C_3N_4-Imine/TiO_2 Nanoparticles, *Inorg. Chem.*, 2021, **60**(13), 9484–9495.

48 M. Jafarpour, A. Rezaeifard, V. Yasinzadeh and H. Kargar, Starch-coated maghemite nanoparticles functionalized by a novel cobalt Schiff base complex catalyzes selective aerobic benzylic C–H oxidation, *RSC Adv.*, 2015, **5**(48), 38460–38469.

49 S. C. Pillai, P. Periyat, R. George, D. E. McCormack, M. K. Seery, H. Hayden, J. Colreavy, D. Corr and S. J. Hinder, Synthesis of high-temperature stable anatase TiO_2 photocatalyst, *J. Phys. Chem. C*, 2007, **111**(4), 1605–1611.

50 Y. Suda and T. Morimoto, Molecularly adsorbed water on the bare surface of titania (rutile), *Langmuir*, 1987, **3**(5), 786–788.

51 E. Wirnhier, M. Döblinger, D. Gunzelmann, J. Senker, B. V. Lotsch and W. Schnick, Poly (triazine imide) with intercalation of lithium and chloride ions $[(C_3N_3)_2(NHxLi1\text{-}x)_3.LiCl]$: a crystalline 2D carbon nitride network, *Chem.–Eur. J.*, 2011, **17**(11), 3213–3221.

52 M. Devi, S. Ganguly, B. Bhuyan, S. S. Dhar and S. Vadivel, A novel [Fe $(acac)_3$] interspersed g-C_3N_4 heterostructure for environmentally benign visible-light-driven oxidation of alcohols, *Eur. J. Inorg. Chem.*, 2018, **2018**(44), 4819–4825.

53 J. Ding, W. Xu, H. Wan, D. Yuan, C. Chen, L. Wang, G. Guan and W.-L. Dai, Nitrogen vacancy engineered graphitic C3N4-based polymers for photocatalytic oxidation of aromatic alcohols to aldehydes, *Appl. Catal., B*, 2018, **221**, 626–634.

54 M. Zhang, C. Chen, W. Ma and J. Zhao, Visible-light-induced aerobic oxidation of alcohols in a coupled photocatalytic system of dye-sensitized TiO_2 and TEMPO, *Angew. Chem., Int. Ed.*, 2008, **47**(50), 9730–9733.

55 F. Su, S. C. Mathew, G. Lipner, X. Fu, M. Antonietti, S. Blechert and X. Wang, mpg-C_3N_4-catalyzed selective oxidation of alcohols using O_2 and visible light, *J. Am. Chem. Soc.*, 2010, **132**(46), 16299–16301.

56 M. Li, S. Wu, X. Yang, J. Hu, L. Peng, L. Bai, Q. Huo and J. Guan, Highly efficient single atom cobalt catalyst for selective oxidation of alcohols, *Appl. Catal., A*, 2017, **543**, 61–66.

57 S. Higashimoto, N. Kitao, N. Yoshida, T. Sakura, M. Azuma, H. Ohue and Y. Sakata, Selective photocatalytic oxidation of benzyl alcohol and its derivatives into corresponding aldehydes by molecular oxygen on titanium dioxide under visible light irradiation, *J. Catal.*, 2009, **266**(2), 279–285.

58 L. Sun, B. Li, X. Chu, N. Sun, Y. Qu, X. Zhang, I. Khan, L. Bai and L. Jing, Synthesis of Si-O-Bridged g-C_3N_4/WO_3 2D-heterojunctional nanocomposites as efficient photocatalysts for aerobic alcohol oxidation and mechanism insight, *ACS Sustainable Chem. Eng.*, 2019, **7**(11), 9916–9927.

59 Y. Shiraishi, H. Sakamoto, Y. Sugano, S. Ichikawa and T. Hirai, Pt-Cu bimetallic alloy nanoparticles supported on anatase TiO_2: highly active catalysts for aerobic oxidation driven by visible light, *ACS Nano*, 2013, **7**(10), 9287–9297.

60 B. Long, Z. Ding and X. Wang, Carbon nitride for the selective oxidation of aromatic alcohols in water under visible light, *ChemSusChem*, 2013, **6**(11), 2074–2078.

61 T. Hille, T. Irrgang and R. Kempe, The synthesis of benzimidazoles and quinoxalines from aromatic diamines and alcohols by iridium-catalyzed acceptorless dehydrogenative alkylation, *Chem.–Eur. J.*, 2014, **20**(19), 5569–5572.

62 Y. Shiraishi, Y. Sugano, S. Tanaka and T. Hirai, One-Pot Synthesis of Benzimidazoles by Simultaneous Photocatalytic and Catalytic Reactions on Pt@TiO_2 Nanoparticles, *Angew. Chem.*, 2010, **122**(9), 1700–1704.

63 K. D. Parghi and R. V. Jayaram, Sequential oxidation and condensation of alcohols to benzimidazoles/benzodiazepines by MoO_3-SiO_2 as a heterogeneous bifunctional catalyst, *Catal. Commun.*, 2010, **11**(15), 1205–1210.

64 H. Wang, J. Zhang, Y.-M. Cui, K.-F. Yang, Z.-J. Zheng and L.-W. Xu, Dehydrogenation and oxidative coupling of alcohol and amines catalyzed by organosilicon-supported TiO_2@PMHSIPN, *RSC Adv.*, 2014, **4**(65), 34681–34686.

65 L. Li, Q. Luo, H. Cui, R. Li, J. Zhang and T. Peng, Air-stable Ruthenium(II)-NNN Pincer Complexes for the Efficient Coupling of Aromatic Diamines and Alcohols to 1H-benzo

[d] imidazoles with the Liberation of H_2, *ChemCatChem*, 2018, **10**(7), 1607–1613.

66 J. Yu, J. Xu and M. Lu, Copper-catalyzed highly efficient aerobic oxidative synthesis of benzimidazoles, benzoxazoles and benzothiazoles from aromatic alcohols under solvent-free conditions in open air at room temperature, *Appl. Organomet. Chem.*, 2013, **27**(10), 606–610.

67 P. L. Reddy, R. Arundhathi, M. Tripathi, P. Chauhan, N. Yan and D. S. Rawat, Solvent-Free Oxidative Synthesis of 2-Substituted Benzimidazoles by Immobilized Cobalt Oxide Nanoparticles on Alumina/Silica Support, *ChemistrySelect*, 2017, **2**(13), 3889–3895.